$[Al_2O_4]^-$, a benchmark gas-phase class II mixed-valence radical anion for the evaluation of quantum-chemical methods

Martin Kaupp,[a,*] Amir Karton,[b] Florian A. Bischoff[c]

[a]Institut für Chemie, Technische Universität Berlin, Theoretische Chemie/Quantenchemie, Sekr. C7, Straße des 17. Juni 135, D-10623, Berlin, Germany, email: martin.kaupp@tu-berlin.de; [b]School of Chemistry and Biochemistry, The University of Western Australia, 35 Stirling Highway, Crawley, Perth, Australia; [c]Humboldt-Universität zu Berlin, Institut für Chemie, Theoretische Chemie/Quantenchemie, Brook-Taylor-Str. 2, 12489 Berlin

Abstract. The radical anion $[Al_2O_4]^-$ has been identified as rare example of a small gas-phase mixed-valence system with partially localized, weakly coupled class II character in the Robin/Day classification. It exhibits a low-lying C_{2v} minimum with one terminal oxyl radical ligand and a high-lying D_{2h} minimum at about 70 kJ/mol relative energy with predominantly bridge-localized-hole character. Two identical C_{2v} minima and the D_{2h} minimum are connected by two C_{2v}-symmetrical transition states, which are only ca. 6-10 kJ/mol above the D_{2h} local minimum. The small size of the system and the absence of environmental effects has for the first time enabled the computation of accurate *ab initio* benchmark energies, at the CCSDT(Q)/CBS level using W3-F12 theory, for a class-II mixed-valence system. These energies have been used to evaluate wave-function-based methods [CCSD(T), CCSD, SCS-MP2, MP2, UHF] and density functionals ranging from semi-local (e.g. BLYP, PBE, M06L, M11L, N12) via global hybrids (B3LYP, PBE0, BLYP35, BMK, M06, M062X, M06HF, PW6B95) and range-separated hybrids (CAM-B3LYP, ωB97, ωB97X-D, LC-BLYP, LC-ωPBE, M11, N12SX), the B2PLYP double hybrid, and some local hybrid functionals. Global hybrids with about 35-43% exact-exchange (EXX) admixture (e.g. BLYP35, BMK), several range hybrids (CAM-B3LYP, ωB97X-D, ω-B97), and a local hybrid provide good to excellent agreement with benchmark energetics. In contrast, too low EXX admixture leads to an incorrect delocalized class III picture, while too large EXX over-localizes and gives too large energy differences. These results provide support for previous method choices for mixed-valence systems in solution, and for the treatment of oxyl defect sites in alumosilicates and SiO_2. Vibrational gas-phase spectra at various computational levels have been compared directly to experiment and to CCSD(T)/aug-cc-pV(T+d)Z data.

Keywords. Aluminum oxide cluster anion, mixed-valence systems, coupled-cluster calculations, electron transfer, delocalization error, surface-defect localization.

1. Introduction

Mixed-valence (MV) systems are characterized by containing the same redox center in different formal oxidation states, and they are important models for (inter- and intramolecular) electron transfer (ET) in a large variety of technologically or biologically important processes. The processes range from charge transfer in organic semiconductors to the well-known inner-sphere processes in transition-metal systems, and for a large range of biological systems. In all of these cases the detailed study of MV compounds is of crucial interest and is done in various ways from electrochemistry to many types of spectroscopy.[1]

Quantum-chemical calculations are an important complement to spectroscopic work in this area, and we have recently reviewed in detail the current scope and limitations of such computational studies.[2] The task at hand is to provide a balanced treatment of localization/delocalization of spin/charge, in particular for systems that are relatively close to the borderline between class II (partially localized) and class III (fully delocalized) in the well-known Robin/Day classification of MV systems.[3] It turns out that both the requirements of the underlying electronic-structure method and the need to incorporate environmental effects into the computational modeling provide substantial challenges to such quantum-chemical work. The electronic-structure methodology needs to provide a sensitive balance between the effects of exchange (minimal self-interaction errors) and the treatment of both dynamical and non-dynamical electron-correlation effects.[4,5] The need to adequately treat the environment arises from the fact that most MV systems of practical interest are anionic or cationic open-shell systems of often appreciable size, which can usually be studied only in polar solvent environments (or in an equally polar solid-state environment). In addition to the effects of the solvent, also the effects of counter-ions may have to be considered, thereby further complicating the computational modeling.

The evaluation of the reliability and predictive quality of quantum-chemical approaches to MV systems close to the class II/III border thus turns into a multi-parameter problem, where a number of aspects have to be carefully controlled simultaneously. Over the past five years, we have evaluated extensively a computational protocol based on density functional theory (DFT), with either global or range-separated hybrid functionals incorporating enhanced exact-exchange admixtures, and implicit solvent models (either dielectric continuum models or the Direct-COSMO-RS approach[5,6]). Successful applications ranging from organic MV systems, such as bis-triaryl-amine radical cations and related systems (also MV cations bridged by transition-metal centers)[4,7] or dinitro-aryl or diquinone radical anions,[5,8] to a wide variety of transition-metal MV complexes,[2,9] have provided evidence for a rather robust performance of these DFT-based protocols. In fact, the treatment of conformational effects on spectroscopic properties revealed that both localized and delocalized portions of a potential-energy surface may contribute to NIR or vibrational spectra.[10]

However, in view of the abovementioned complications arising from the treatment of environmental effects, the possibility of fortuitous error compensation cannot be ruled out completely. Other approaches to the electronic structure-problem (e.g. tuned range hybrids[11]) or to the treatment of environmental effects (e.g. QM/MM molecular dynamics approaches[12] or the RISM-SCF model[13]) have been put forward. We note also, that some previous method evaluations have compared gas-phase calculations to condensed-phase experimental data which are expected to be heavily influenced by the environment,[14] or to *ab initio* benchmark data that may not have been converged sufficiently in terms of one-particle basis sets.[15]

To be able to establish with greater certainty the performance of different electronic-structure methods without the complication of environmental effects, small gas-phase MV systems, for which experimental and/or highly accurate theoretical benchmark data are

available, would be highly useful. Unfortunately, in the absence of a polar environment most of the smaller MV systems tend to be delocalized class III systems, as strong electronic coupling over short distances between two redox centers leads to symmetrical delocalization of spin and charge densities. The title system of the present work, the small gas-phase radical anion $[Al_2O_4]^-$, is a notable exception: its vibrational spectrum has recently been characterized[16] by cryogenic ion-trap mass-spectrometry-based infrared-predissociation (IR-PD) spectroscopy, and comparison of calculated and experimental spectra clearly indicates the system to have a C_{2v}-symmetrical structure with class-II character. Moreover, its small size makes this radical anion an ideal target for accurate benchmark post-HF methodology, thus providing the needed accurate reference data.

In addition to being a prototypical, general class-II MV system, the title anion is also more directly relevant as an interesting and useful small model for electron-hole defect localization in oxide solids and surfaces. In particular, the electronic-structure situation relates closely to $[AlO_4]^0$ point defects in alumosilicates and to "non-bridging-oxygen" Si-O· radical surface defects in SiO_2. These are of importance, for example, in the context of EPR or optical studies of zeolites and α-silica, or in the toxicity of microcrystalline silica forms. In both cases, previous DFT studies[17] have exposed deficiencies in standard exchange-correlation functionals regarding localization of the electron hole on one oxygen p-orbital, whereas approaches with reduced self-interaction errors perform notably better.

2. Computational Details

The calculations have been performed with a local development version of the Turbomole (revision 6.6),[18] Gaussian09 (revisions A.02 and D.01),[19] as well as with the MOLPRO (revision 2012.1)[20] and MRCC[21] program suites. We have ensured that the

programs provide identical energies (to within less than 0.1 mH) and structures (to within less than 0.005 Å) at a given computational level.

High-level benchmark data have been obtained using W3-F12 theory.[22] W3-F12 theory (and its earlier version W3.2 theory[23]) represent layered extrapolations to the all-electron CCSDT(Q)/CBS limit and can achieve 'near-benchmark accuracy' for atomization reactions (i.e., they are associated with root-mean-square deviations, RMSDs, from accurate atomization energies of about 1 kJ/mol).[22] For example, W3-F12 theory is associated with an RMSD of 1.1 kJ/mol for a set of 140 very accurate atomization energies obtained at the full configuration interaction (FCI) infinite basis-set limit.[22,23] W3-F12 theory combines F12 methods[24] with basis-set extrapolations in order to reproduce the CCSDT(Q)/CBS energy.[25] In W3-F12, the CCSD(T)/CBS energy is obtained from W2-F12 theory,[22] and the post-CCSD(T) contributions are obtained from W3.2 theory[23]. In brief, the Hartree–Fock (ROHF) component is calculated with the cc-pVQZ-F12 basis set of Peterson *et al.* which were developed for explicitly correlated calculations.[26] Note that the complementary auxiliary basis (CABS) singles correction is included in the SCF energy.[27,28,29] The valence CCSD-F12 correlation energy is extrapolated from the cc-VTZ-F12 and cc-VQZ-F12 basis sets, using the $E(L) = E_\infty + A/L^\alpha$ two-point extrapolation formula, with $\alpha = 5.94$. In all of the explicitly-correlated coupled cluster calculations the diagonal, fixed-amplitude 3C(FIX) ansatz[28,30] and the CCSD-F12b approximation[29,31] are employed. The quasiperturbative triples, (T), corrections are calculated with the cc-pVTZ-F12 basis set and scaled by the factor $f = 0.987 \times E^{MP2\text{-}F12}/E^{MP2}$. This approach has been shown to accelerate the basis-set convergence.[22,31] The post-CCSD(T) corrections are obtained from standard coupled-cluster calculations (i.e., without inclusion of F12 terms). Specifically, the higher-order connected triples (CCSDT-CCSD(T)) valence correlation contribution is extrapolated from the cc-pVDZ and cc-pVTZ basis sets using the above two-point extrapolation formula with $\alpha = 3$. The parenthetical

connected quadruples contribution (CCSDT(Q)-CCSDT) is calculated with the cc-pVDZ basis set[23]. The CCSD inner-shell contribution is calculated with the core-valence weighted correlation-consistent aug-cc-pwCVTZ basis set of Peterson and Dunning,[32] whilst the (T) inner-shell contribution is calculated with the cc-pwCVTZ basis set without the *f* functions.[22] Finally, in order to assess the quality of the BLYP35/def2-TZVP structures (C_{2v} and D_{2h} minima and C_{2v} transition state, cf. Figure 1) employed for the single-point WF calculations, we also optimized the structures of the minima at the CCSD(T)/aug-cc-pVQZ level of theory.

Preceding these W3-F12 benchmarks, we had also computed single-point energies [MP2, SCS-MP2, MP4(SDQ), CCSD, CCSD(T)] based on UHF reference wave functions with aug-cc-pVXZ (X = T, Q, 5) correlation-consistent basis sets,[33] at the abovementioned BLYP35/def2-TZVP structures, using the frozen-core approximation (with a [He] core for Al and O) and subsequent extrapolation to the complete-basis-set limit (CBS) using the two-point formula of Halkier et al.[34] with either X = T, Q or X = Q, 5 (due to computational limitations, CCSD(T) data are provided only for X = T, Q). Results will be reported in Supporting Information.

The abovementioned benchmark data were used to evaluate the performance of a large variety of different DFT approaches to correctly describe the relative energies of the minima. The DFT calculations were used to optimize both the C_{2v} and D_{2h} minimum structures, and in selected cases also the transition state. The DFT calculations used def2-TZVP basis sets.[35] Test calculations with the BLYP35 functional[4,5] (derived from the BHandHLYP[36] or B1LYP[37] functional form but with the EXX admixture fixed to 35%) and a larger def2-QZVP basis set[35] confirmed that DFT energies at def2-TZVP level are converged within ca. 1 kJ/mol (except possibly for the B2PLYP double-hybrid functional tested) and interatomic distances to within 0.002 Å. Smaller def2-SVP basis sets[38] lead to larger deviations. An intrinsic reaction coordinate (IRC) scan[39] at BLYP35/def2-TZVP level (see Figure 1 for the energy

profile) confirmed that the transition state indeed connects the two minima studied. As electron transfer from one terminal oxo group to the electron-deficient terminal oxyl group on the opposite side of the C_{2v} minimum generates an identical C_{2v} minimum, the system may be described by a triple-well ground-state potential-energy curve (Figure 1; see discussion of the electronic-structure implications further below). The transition state has been located by first carrying out a relaxed scan of the Al-Al distance, starting from the high-lying local D_{2h} minimum. The structure that immediately preceded the relaxation to the global C_{2v} minimum was used as starting point for a regular transition-state optimization (Berny algorithm, opt=TS keyword in Gaussian09). Stationary points at most levels have been characterized by harmonic vibrational frequency analyses.

The use of different quantum-chemical program packages has been motivated by the availability of different varieties of exchange-correlation functionals that we could thereby compare. In the locally modified Turbomole version, we have used not only B1LYP-type functionals with variable exact-exchange admixture, and the PW6B95 global hybrid,[40] advocated recently for its particularly robust performance for main-group energetics,[41] but we also performed preliminary calculations with some local hybrid functionals incorporating position-dependent exact-exchange admixture. Only one type of simple local hybrids has been evaluated, based on only LSDA (Slater) and exact exchange and LSDA (PW92[42]) correlation and a simple local mixing function[43] (LMF) $a(\mathrm{r}) = b\tau_W/\tau$ (τ_W is the von Weizsäcker kinetic energy density and τ the Kohn-Sham local kinetic energy density; this type of LMF is termed *t*-LMF), without calibration[44] of exchange-energy densities. Self-consistent structure optimizations used a recently reported, efficient semi-numerical Turbomole implementation,[45] augmented by analytical gradients for structure optimization (Klawohn, S.; Bahmann, H.; Kaupp, M., manuscript in preparation).

Gaussian09 provided in turn access to a large variety of further exchange-correlation functionals. The functionals evaluated in this case ranged from semi-local functionals (BLYP,[46] PBE[47], M06L,[48] M11L[49], N12[50]) via global hybrids (B3LYP,[51] PBE0,[52] PBE0-1/3,[53] BLYP35, BMK,[54] M06,[55] M062X,[55] M06HF[56]) and range-separated hybrids (CAM-B3LYP,[57] ωB97,[58] ωB97X-D,[59] LC-BLYP,[60] LC-ωPBE,[61] M11,[62] N12SX[63]) to the B2PLYP double hybrid.[64] Of these functionals, only ωB97X-D includes explicit dispersion corrections. The latter are, however, expected to be of little importance for the title system due to its small size and "hard" electrostatic bonding type. We used generally default thresholds for convergence of structure optimizations and for vibrational frequency calculations in the Gaussian09 and Turbomole codes.

Based on these data, structures and spin-density distributions were visualized using the Chemcraft software.[65] Mulliken atomic spin densities and natural-population-analysis[66] (NPA) atomic charges were computed to assist electronic-structure analyses.

3. Results and Discussion

Electronic-structure considerations. We start by analyzing the molecular and electronic structure of the C_{2v} and D_{2h} minima and of the transition state interconverting them, mainly to know what computational challenges to expect. We use here the results obtained with the BLYP35 and BMK global hybrid functionals, and with the CAM-B3LYP and ωB97X-D range hybrids. These functionals turn out to provide energetics that agree well with CCSDT(Q)/CBS benchmark data (see further below). The energy profile in Figure 1, obtained from an IRC scan at BLYP35/def2-TZVP level (with relative energies of stationary points also provided for BMK, CAM-B3LYP and ωB97X-D), provides closer understanding. For a partially localized class II MV system, a two-state scenario by electronic coupling of two

localized diabatic states would predict a double-well adiabatic ground-state potential with two identical minima of lower symmetry (in the present case C_{2v}), connected by a transition state for thermal electron transfer (in the present case of D_{2h} symmetry). This is not quite borne out by Figure 1, as the D_{2h}-symmetrical, energetically high-lying structure is actually a very shallow minimum, with very small barriers of about 6-10 kJ/mol connecting it to the two identical low-lying C_{2v} minima. This can be understood within the framework of a three-state scenario (in a generalized Mulliken-Hush formalism), where a high-lying bridge-localized state[1a,67] mixes in at D_{2h} symmetry, thereby slightly stabilizing the high-symmetry structure, to the extent that it becomes a local minimum. Indeed, the spin-density distributions show that, while the electron hole (compared to a closed-shell dianion with $2xAl^{3+}$ and $4xO^{2-}$ description) is localized at either one of the two terminal oxygen ligands at the two equivalent C_{2v} minima (Figure 2a), it has largely shifted to the two bridging oxygen atoms at the D_{2h} local minimum (Figure 2b). This is also apparent from the Mulliken atomic spin densities, and the oxyl vs. oxo ligand character of the different structures is also reflected in NPA charges (see Table S1 in Supporting Information).

As a consequence, one of the two terminal Al-O bonds is considerably lengthened in the C_{2v} structure (Figure 1), consistent with a terminal oxyl radical. In contrast, the hole at the bridging positions in the local D_{2h} minimum reduces the electrostatic attraction in the center of the anion and thereby leads to a substantial lengthening of the Al-Al distance from about 2.4 Å to about 2.8 Å (Figure 1). The C_{2v}-symmetrical transition state (TS) deviates only moderately from the D_{2h} local minimum, with the Al-Al distance contracting to about 2.7 Å and the two terminal Al-O distances becoming slightly nonequivalent. Indeed, the spin density at the TS is delocalized between one of the terminal and both bridging oxygen atoms (Figure 2c, Table S1). We note in passing, that in addition to the ET and MV aspects of this system, the high-lying bridge-localized D_{2h} minimum may be viewed as a bond stretch isomer

of the low-lying C_{2v} minima (in analogy to transition-metal[68] and main-group systems[69] with comparable bicyclobutane-type cores), as the overall connectivity remains identical. We may furthermore link the differences between a localized oxyl radical in the low-lying C_{2v} minima and the more delocalized situation at the high-lying D_{2h} minimum to prototypical situations in small-molecule activation:[70] it is known that the larger spin density on the localized radical oxygen atom is better poised towards, e.g., C-H activation than the lower spin density of a delocalized case.

This qualitative bonding situation is obtained at all computational levels that provide realistic energy profiles (see below). In contrast, due to extensive delocalization errors, all semi-local DFT functionals give only essentially one D_{2h} symmetrical structure (but see discussion below), in which the spin density is symmetrically delocalized onto the two terminal oxygen atoms (cf. Figure 2d), leading to expanded, equal terminal Al-O distances and to a short Al-Al distance (see below). At intermediate EXX admixtures, a high-lying bridge-localized D_{2h} minimum with long Al-Al distance and a low-lying minimum with short Al-Al distance and spin density at the terminal oxygen atoms both exist, but the latter now becomes almost or exactly D_{2h} symmetrical as well (see below).

We also note that the ca. 68 kJ/mol relative energy of the D_{2h} local minimum and the further ca. 8 kJ/mol at the TS (Figure 1) characterize this system as a weakly coupled class II system, close to the class II/I borderline. This is particularly remarkable given that these are gas-phase data. Activation barriers of more strongly coupled class II systems, which we have studied computationally in polar solvent environments, typically range from 10 kJ/mol to 30 kJ/mol.[2,4,5] The weak electronic coupling in such a small radical anion may seem surprising at first sight, given the short distance of only about 5.8 Å between the two terminal oxygen atoms, between which the ET largely occurs. It appears that the large Al-O bond

ionicity (cf. NPA charges in Table S1) is responsible for the relatively weak electronic interaction.

Benchmark *ab initio* energies. Table 1 gathers the component breakdown of the W3-F12 energy separations between the C_{2v} and D_{2h} local minima ($\Delta E(D_{2h}\text{-}C_{2v})$) and the D_{2h} local minimum and the C_{2v} TS ($\Delta E(TS\text{-}D_{2h})$). For the $\Delta E(D_{2h}\text{-}C_{2v})$ energy gap we have W3-F12 results for both the CCSD(T)/aug-cc-pVQZ and BLYP35/def2-TZVP reference structures. Inspection of Table 1 reveals that there is some reshuffling between the SCF and CCSD correlation energies due to the structural change. In particular, the SCF energy obtained with the BLYP35 reference geometry is lower by 0.9 kJ/mol than that obtained with the CCSD(T) geometry, whereas the CCSD correlation component obtained with the BLYP35 geometry is higher by 0.8 kJ/mol than that obtained with the CCSD(T) structure. The differences in the (T) and core-valence components between the two structures also cancel each other out to a large extent (Table 1). The difference in geometries has practically no effect on the post-CCSD(T) contributions. Overall, the difference in the all-electron CCSDT(Q)/CBS energies between the BLYP35 and CCSD(T) structures is merely 0.1 kJ/mol. This small difference indicates that the BLYP35 structures are adequate for describing the energetics of the $[Al_2O_4]^-$ systems.

Let us now turn to the W3-F12 components of the $\Delta E(D_{2h}\text{-}C_{2v})$ energy gap obtained with the BLYP35/def2-TZVP structures (Table 1). At the ROHF/CBS level of theory this energy separation is grossly overestimated at 207.2 kJ/mol. The valence CCSD component reduces this energy gap by 117.0 kJ/mol, and the (T) component reduces it further by 20.9 kJ/mol. Taking into account the very small core-valence contribution of +0.1 kJ/mol, we obtain $\Delta E(D_{2h}\text{-}C_{2v})$ = 69.5 kJ/mol at the all-electron CCSD(T)/CBS level of theory. The higher-order connected triples, T_3-(T), correlation contribution amounts to +1.5 kJ/mol, whilst the parenthetical connected quadruple excitations, (Q), contribution amounts to -3.0 kJ/mol.

Overall, the post-CCSD(T) contributions reduce the $\Delta E(D_{2h}\text{-}C_{2v})$ energy gap by a relatively modest amount of 1.5 kJ/mol. Moving on to the $\Delta E(TS\text{-}D_{2h})$ energy separation, again the HF/CBS level of theory represents an overestimation with $\Delta E(TS\text{-}D_{2h})$ = 12.7 kJ/mol. The valence CCSD and (T) components reduce this energy gap by 2.6 and 1.1 kJ/mol, respectively, and the core-valence contribution reduces it further by 0.8 kJ/mol. Thus, at the all-electron CCSD(T)/CBS level of theory we obtain $\Delta E(TS\text{-}D_{2h})$ = 8.1 kJ/mol. The post-CCSD(T) contributions tend to largely cancel one another (namely, the T_3-(T) and (Q) contributions are -2.6 and +2.1 kJ/mol, respectively). Our best all-electron CCSDT(Q)/CBS energy gaps from W3-F12 theory are: $\Delta E(D_{2h}\text{-}C_{2v})$ = 67.9 kJ/mol and $\Delta E(TS\text{-}D_{2h})$ = 7.6 kJ/mol.

Tables S2 and S3 in Supporting Information provide further (in this case UHF-based) CBS-extrapolated *ab initio* energy differences between the high-lying local D_{2h} and the low-lying C_{2v} minimum obtained in single-point calculations at BLYP35/def2-TZVP-optimized structures, as well as between the D_{2h} minimum and the transition state. The relatively large contribution from CCSD(T) triple excitations is again notable. It reflects appreciable non-dynamical correlation contributions for this geometry. We note that the valence CCSD(T)/$CBS_{TZ\text{-}QZ}$ $\Delta E(D_{2h}\text{-}C_{2v})$ and $\Delta E(TS\text{-}D_{2h})$ values (70.2 and 9.1 kJ/mol, respectively) are in very good agreement with the corresponding values from W2-F12 theory (69.1 and 9.0 kJ/mol, respectively).

Consistent with the relatively modest post-CCSD(T) contributions (Table 1), we do not see any indications for a breakdown of the single-reference coupled-cluster methodology. Depending on basis sets, D1 diagnostics[71] range from 0.060-0.065 for the C_{2v} minima and from 0.056-0.059 for the D_{2h} minimum. That is, the D_{2h} minimum in each case exhibits actually a slightly *smaller* value! There is no clear consensus on the D1 values at which a multi-reference character starts to be dominant. In particular this is not very well established

for open-shell cases. In case of transition-metal systems, it has been argued that D1 diagnostics as large as 0.15 may delineate the breakdown of single-reference methods,[72] and Grimme has used a value of 0.10 to exclude systems from judging DFT approaches by CCSD(T) benchmarks.[73] Feller and Peterson[74] analyzed the situation for the HO_2 and C_2 radical systems, which exhibited D1 values of 0.126 and 0.087, respectively, and they found no indications for a breakdown of single-reference coupled-cluster methods. The $\%TAE_e[(T)]$ diagnostics for the importance of non-dynamical correlation effects,[23] i.e. the percentage of the total atomization energy accounted for by parenthetical connected triple excitations, range between 3.2% (C_{2v} minimum) and 4.1% (D_{2h} minimum and TS). Consistent with the above W3-F12 results, these $\%TAE_e[(T)]$ values also indicate that the $[Al_2O_4]^-$ system is characterized by notable but mild non-dynamical correlation effects. Spin contamination is also not very serious. UHF wave-functions have S^2 expectation values of around 0.758 for the C_{2v} minima and up to 0.801 for the D_{2h} minimum. In our experience, these are values that are easily corrected for at unrestricted CCSD(T) level.[75] As expected, the DFT approaches exhibit significantly lower S^2 expectation values than UHF, of course depending on the amount of exact-exchange admixture in the functional. We conclude that the triples contributions provide an important stabilization of the D_{2h} local minimum (and the TS), but single-reference coupled-cluster approaches are adequate benchmark tools in the present case.

MP2 underestimates the CCSD(T) energy difference by only about 5 kJ/mol (Table S2). This relatively good MP2 performance is likely due to a compensation of errors (lack of triple excitations, overshooting of double-excitation contribution). In this case, spin scaling (SCS-MP2) shifts the energy difference up to about 80 kJ/mol, into the middle between the CCSD and CCSD(T) results.

Evaluation of different exchange-correlation functionals for energies and minimum structures. Table 2 compares the energy difference between D_{2h} and C_{2v} structures and some

crucial structure parameters (Al-Al distance for both C_{2v} and D_{2h} optimizations, asymmetry of the two terminal Al-O distances in the C_{2v} minimum) obtained with one-parameter hybrid functionals of the BHLYP (or B1LYP) type, where only the exact-exchange (EXX) admixture is varied (more details are provided in Table S4 in Supporting Information). Previous experience of such evaluations for organic MV systems in solution (i.e. using continuum solvent models in the structure optimization) indicated that semi-local functionals and global hybrid functionals with less than 30% EXX admixture give delocalized symmetrical structures even in cases where experimental evidence pointed to a localized class II situation.[2]

These delocalization errors of standard functionals are clearly confirmed for the present gas-phase example (see also Figure 3): while optimizations with the BLYP-based functionals up to 25% EXX admixture in C_{2v} and D_{2h} symmetry, respectively, still provide two different structures and an energy difference of about 20 kJ/mol in favor of the C_{2v} optimization, closer inspection shows that even the latter is close to D_{2h}. In fact, the differences between the two structures are rather minor and may reflect the limits of the structure optimization for the (unrealistically) shallow potential-energy surfaces in these cases. The situation changes sharply between 25% and 26% EXX admixture (Table 2, Figure 3): now the energy difference jumps to about 80 kJ/mol, and the high-lying D_{2h} structure has developed the bridge-localized character with long Al-Al distance (see above). However, the low-lying C_{2v} minimum is still very close to a D_{2h}-symmetrical situation with the spin density symmetrically distributed over the two terminal oxygen atoms (as indicated by the short Al-Al and two long terminal Al-O distances). For this low-lying minimum, localization of the spin onto only one of the terminal ligands, accompanied by clearly distinct terminal Al-O distances, occurs rather sharply at about 33% EXX admixture (Table 2, Figure 3). We can thus see two "jumps" in the features related to delocalization errors: large delocalization errors make the high-lying bridge-localized D_{2h} structure vanish, and only a structure with half of a hole on the two

terminal oxygen atoms is retained. At intermediate EXX admixtures, the bridge-localized D_{2h} structure appears at high energies, but the low-lying minimum still exhibits delocalization of the hole between the two terminal oxygen ligands and is close to D_{2h}. Only upon further reduction of delocalization errors, the qualitatively correct situation emerges, with a high-lying bridge-localized D_{2h} minimum and a low-lying, symmetry-broken C_{2v} minimum with clear localization of the hole onto only one of the two terminal oxygen atoms. Further increase of EXX admixture retains a qualitatively correct picture but increases the D_{2h}-C_{2v} energy differences further, leading to an overestimate compared to the CCSDT(Q)/CBS reference value. The polarization of spin onto one side of the system is also further enhanced. This "over-localization" then peaks in UHF calculations (see above), where electron correlation lacks completely.

Closer examination of the results obtained with the various functionals reveals some further aspects (Table 3, Figure 4): a) Those range-separated hybrids that most successfully reproduce the benchmark CCSDT(Q)/CBS data are CAM-B3LYP and ωB97X-D. These two functionals share a similar finite amount of EXX admixture at short range (19% and 22%, respectively)[57,58] but differ in the long-range contribution (65% and 100%, respectively). ωB97 is still rather close to the reference energetics, whereas M11, LC-BLYP, and LC-ωPBE belong to those functionals that overlocalize. In the latter two cases, similar behavior had also been found already for organic MV radical anions in solution.[5,8] M11 features relatively high EXX (42%) already at short range,[62] whereas the other three functionals interpolate between 0% and 100%. While N12SX is also technically a range hybrid, it belongs to the subclass of screened-exchange hybrids, i.e. it has 0% EXX at long range and 25% EXX at short range. While such functionals can be advantageous for solid-state calculations,[76] it is clear that the lack of long-range EXX admixture is unfavorable with respect to delocalization errors. This is

confirmed here, as N12SX performs comparably to semi-local functionals or to global hybrids with low EXX admxiture (Table 3).

We also note that both M06 and PW6B95 belong to the class of global hybrid functionals with insufficient elimination of delocalization errors, giving a delocalization over both terminal oxygen atoms and lacking a bridge-localized minimum (Table 3). This should not be surprising given that these two meta-GGA global hybrids have only 27 % (M06) and 29 % (PW6B95) EXX admixture, respectively. We note, however, that PBE0 with 25% EXX admixture already exhibits the bridge-localized minimum (Table 3). As an alternative parameterization of the latter functional with 33.33% EXX admixture (PBE0-1/3 functional, EXX admixture justified by theoretical considerations[77]) has recently been found to provide even somewhat better thermochemistry and clearly better barriers than the more well-known PBE0 functional,[53] we also included this functional and indeed find a good description of the three-well potential energy surface, as well as reasonable structural data (Table 3; further tests show that the switch in behavior occurs between 30% and 32% EXX admixture, very slightly earlier than for the B1LYP form).

It is also instructive to look at the performance of the B2PLYP double hybrid: this functional provides very reasonable structural parameters for both the C_{2v} and D_{2h} minima (Table 3, Figure 4) but an appreciable underestimate of the energy difference, in spite of its relatively large EXX admixture of 53%. The reason is the MP2-type correlation correction included in the functional, which reduces the energy difference from 104.9 kJ/mol to 54.5 kJ/mol. This is consistent with the larger nondynamical correlation contributions at the bridge-localized D_{2h} structure, which in conjunction with the relatively small occupied/virtual MO energy difference of B2PLYP (compared to HF) leads apparently to a too large MP2 correction. Similar behavior has been found for MV dinitroaryl radical anions in solution.[5]

Results of some exploratory calculations using a series of simple local hybrid functionals based on LSDA only, with a simple scaled *t*-LMF ($b\tau_W/\tau$; see Computational Details), are provided in Table S6 in Supporting Information. Thermochemical optimization of these simplest local hybrids had previously afforded $b = 0.48$ as optimal value.[43] The resulting functional correctly provides a bridge-localized D_{2h} minimum. However, the "C_{2v} minimum" exhibits almost no symmetry breaking, and the energy difference between the two minima is appreciably underestimated (Table S6), comparable to the B3LYP results. A value $b = 0.60$ gives a more realistic energy difference but also a too delocalized low-energy structure. There is a further sharp switch between $b = 0.64$ and $b = 0.65$. The latter value provides finally a correct symmetry-broken C_{2v} minimum and a very realistic C_{2v}/D_{2h} energy difference compared to the CCSDT(Q)/CBS reference data. A functional with $b = 0.70$ appears to already over-localize slightly (Table S6). Data for the functional with $b = 0.65$ are included in Table 3. We note that a local hybrid with the same *t*-LMF and $b = 0.646$ has been found previously to provide accurate thermochemistry and barriers when used with range separation and partial short-range self-interaction corrections of the LSDA correlation.[78] Implementation of such modified correlation functionals into the analytical gradient program for local hybrids is currently carried out in the TU group. Single-point energies computed with this functional at the structure optimized with $b = 0.65$ (see above) give a C_{2v}/D_{2h} energy difference of 71.3 kJ/mol, in excellent agreement with the W3-F12 benchmark data.

Comparison of key structural parameters to the CCSD(T)/ aug-cc-pVQZ data (cf. Table 2, bottom, and Table S4) indicates overall good agreement for those functionals that provide the qualitatively correct C_{2v} and D_{2h} minima. Most of these functionals (e.g. BLYP35, ωB97X-D, BMK, CAM-B3LYP) give somewhat too short Al-Al and Al-O distances (typically by up to 0.02 Å), and also a slightly too large asymmetry between the two terminal Al-O distances in the C_{2v} minima. Some functionals with less accurate relative energies actually perform

somewhat better for the distances, e.g. M06HF, M11, and the B2PLYP double hybrid. Notably, the local hybrid functional that provides closest agreement with the benchmark energetics ($a(\mathbf{r}) = 0.65$ ◘$_W$/◘) also agrees remarkably well with the CCSD(T) reference structures (Table S5).

Transition state and energy profiles. Figure 1 provides also relative energies of the TS for further functionals, for which the TS could be located. Obviously, the differences between the different functionals remain minor. They all provide activation barriers, starting from the D_{2h} minimum, in the range of 6-8 kJ/mol. This compares well with the ca. 7.6 kJ/mol single-point CCSDT(Q)/CBS reference value (cf. Table 1). The TS structural features of the various optimizations also differ very little from the BLYP35 data shown in Figure 1 (cf. Table S7 in Supporting Information). We could so far not find the TS for functionals that give higher D_{2h} vs. C_{2v} energy differences, but harmonic vibrational frequency analyses characterize the high-lying D_{2h} structure as a local minimum also in these cases (e.g. BHandHLYP, M06-2X, M06-HF, HF).

Vibrational frequencies, comparison with experiment. The experimental evidence for a C_{2v} structure of the title radical anion in the gas phase has been obtained by infrared pre-dissociation (IR-PD) spectroscopy of cryogenically cooled, mass selected ions, combined with initial quantum-chemical calculations.[16] Figure 5 shows that only C_{2v} minima provide reasonable agreement with experiment. Computations with semi-local functionals like PBE, which give D_{2h}-type structures with short Al-Al distance and spin density symmetrically delocalized onto the two terminal oxygen atoms (cf. Figure 2), provide only four bands in the experimentally covered range, while experimentally, six distinct bands at 546 cm^{-1}, 606 cm^{-1}, 711 cm^{-1}, 850 cm^{-1}, 913 cm^{-1}, and 1024 cm^{-1} are observed (Table 4). These are better reproduced by computations at the low-lying C_{2v} minima for some of the functionals that provide a correct energy profile (cf. Figure 1): all seven bands are nicely reproduced by the

range hybrids CAM-B3LYP and ωB97X-D (Figure 5), with a somewhat too low intensity of the highest-energy band and only slightly overestimated frequencies. BMK provides even somewhat better frequencies, but now the relative intensities of the two highest-frequency bands are clearly too low compared to the experimental spectrum (and the band near 550 cm^{-1} is too intense; Table 4, Figure S1 in SI). This becomes so pronounced with the BLYP35 (Figure S1) and PBE0-1/3 global hybrid functionals, that the highest-energy band at 1069 cm^{-1} obtains too low intensity to be visible in the plot (moreover, the two next bands become almost degenerate near 870 cm^{-1}; Table 4). To exclude deviations due to the harmonic approximation from the comparison (which were found to be small at BHandHLYP level, data not shown), we may compare instead against harmonic frequencies obtained at CCSD(T) level (Table 4). The latter agree very well with experiment and provide a good benchmark.

Interestingly, MP2 and double-hybrid B2PLYP calculations provide excellent agreement with the coupled-cluster data (Table 4, Figure S2 in SI), even though the latter method clearly underestimates the energy of the high-lying D_{2h} minimum. The perturbation treatment obviously performs much better near the C_{2v} minima. The MP2 calculations perform better than B2PLYP for the energetics (they are probably favored by some error compensation; see above and Tables 3, S3) and also provide excellent vibrational data. Qualitatively reasonable spectra but with a more pronounced overestimate of the frequencies are found for functionals with "overlocalization" and larger energy differences, such as BHandHLYP and M06-2X (Table 4, Figure S2). We note that the last four methods (B3PLYP, MP2, M06-2X, BHandHLYP) also appear to have some problems with the relative intensities of the three bands at highest energies (Table 4, Figure S2). Unsurprisingly, computations at the high-lying D_{2h} minimum provide in general spectra in poor agreement with experiment for all of the relevant functionals.

4. Conclusions

The $[Al_2O_4]^-$ radical anion has provided the opportunity to study for the first time, by a large range of quantum-chemical methodologies, a clear-cut gas-phase mixed-valence system with Robin/Day class II character, which is also closely related to hole localization in oxide materials and surfaces (see Introduction). The system has a high-lying high-symmetry (D_{2h}) local minimum rather than a transition state connecting the two lower-symmetry minima (C_{2v}). This is due to substantial mixing with a bridge-localized state. A triple-well potential-energy curve results.

The importance of this study arises from the fact that this molecular anion is sufficiently small to allow virtually exact basis-set limit CCSDT(Q) (W3-F12) benchmark calculations of the relative energies of different structures. We have thus been able to evaluate, against these benchmark data, a wide range of quantum-chemical methods, including both post-HF and many DFT approaches, without the additional complication of having to deal with environmental effects. The high-lying D_{2h} minimum exhibits larger non-dynamical correlation effects than the low-lying C_{2v} minimum, as indicated by a substantial reduction of the energy difference by triple excitations at CCSD(T) level. MP2 performs surprisingly well, likely due to error compensation. SCS-MP2 provides energies that are between the respective CCSD and CCSD(T) values. In spite of the appreciable importance of the triple excitations, the title system is not in any way a principal problem for single-reference CCSD(T).

It turns out that the performances of different exchange-correlation functionals follow the trends we had previously obtained for a wide range of organic and transition-metal mixed-valence systems in polar solvents. This provides additional support for the computational protocols developed so far, and indirectly for a rather good performance of the previously applied solvent models. Exact-exchange admixture is the decisive parameter in most cases, and we have identified both global hybrids with 33-43% exact exchange (e.g. BLYP35,

PBE0-1/3, and BMK) and range hybrids like CAM-B3LYP and ωB97X-D as adequate approximations, with the latter two clearly outperforming the global hybrids for the vibrational spectra. Similar functionals are expected to perform well also for the description of localized hole-defects in oxides. Preliminary calculations with a set of simple local hybrid functionals suggest that this type of approach may also be very well suitable for such problems. While functionals with more exact-exchange admixture should also provide the correct localization and possibly good vibrational frequencies, they will likely overestimate barriers for hole transfer and may also be less accurate for other properties, and they will likely overlocalize cases just on the delocalized side of the border between class II and class III.

Acknowledgments. Funding from DFG project KA1187/13-1 and from SFB 1109 (projects A03 and D02) is acknowledged. MK thanks S. Klawohn and H. Bahmann for their work on the gradient code for local hybrid functionals. We are also grateful to Knut R. Asmis for providing the experimental vibrational spectrum from ref. 16 in advance of publication.

Supporting Information. Tables and Figures with additional computational data, and full citations of refs. 19-21. This material is available free of charge via the Internet at http://pubs.acs.org.

Figures

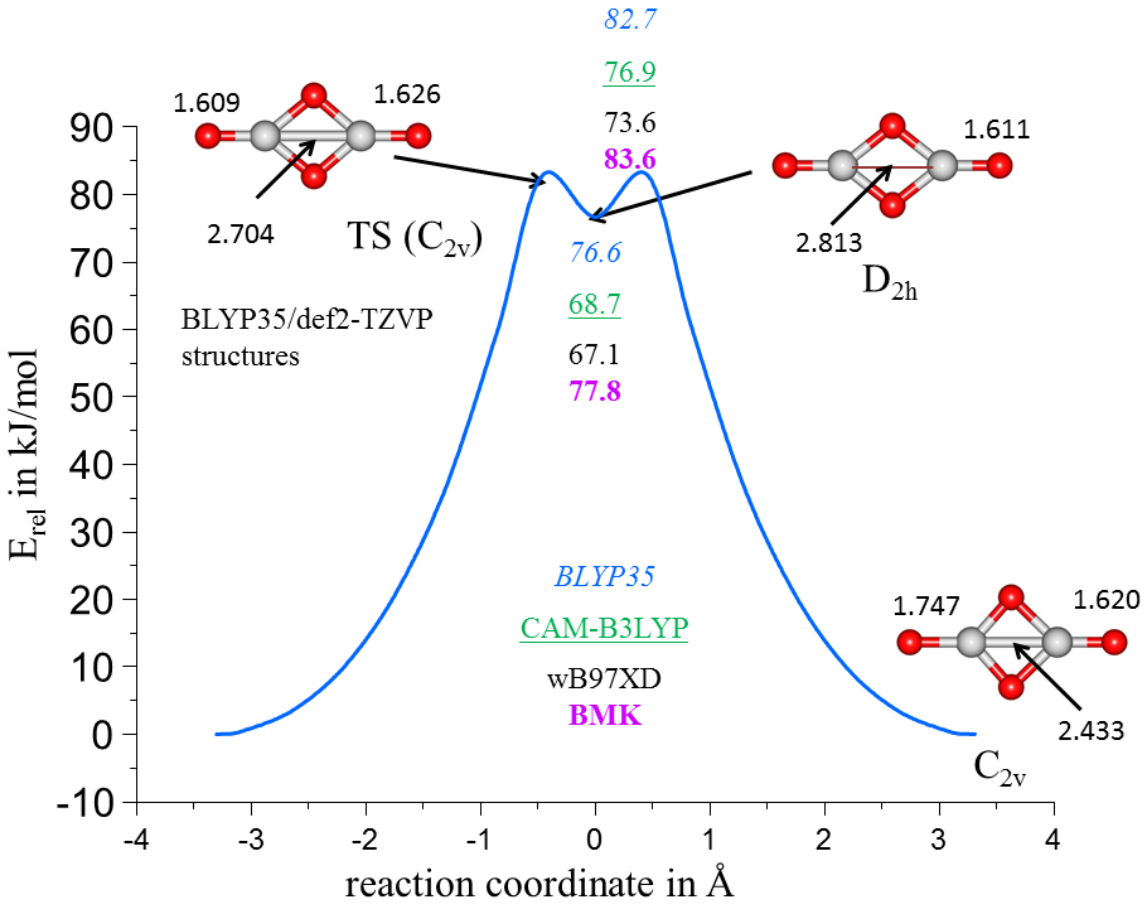

Figure 1. Computed energy profile for the C_{2v}-D_{2h}-C_{2v} electron-transfer reaction of $[Al_2O_4]^-$. The plotted curve and the structural parameters are those obtained at BLYP35/def2-TZVP level. Between the transition states and the C_{2v} minimum, the curve corresponds to an intrinsic reaction coordinate scan (IRC). Due to the shallowness of the potential energy surface between the transition state and the D_{2h} minimum, the IRC did not converge for this direction, and the curve has been completed by a simpler interpolation. Relative energies of stationary points are also provided for the CAM-B3LYP/def2-TZVP, ωB97X-D/def2-TZVP, and BMK/def2-TZVP levels. See Table 1 for the CCSDT(Q)/CBS (W3-F12) reference data.

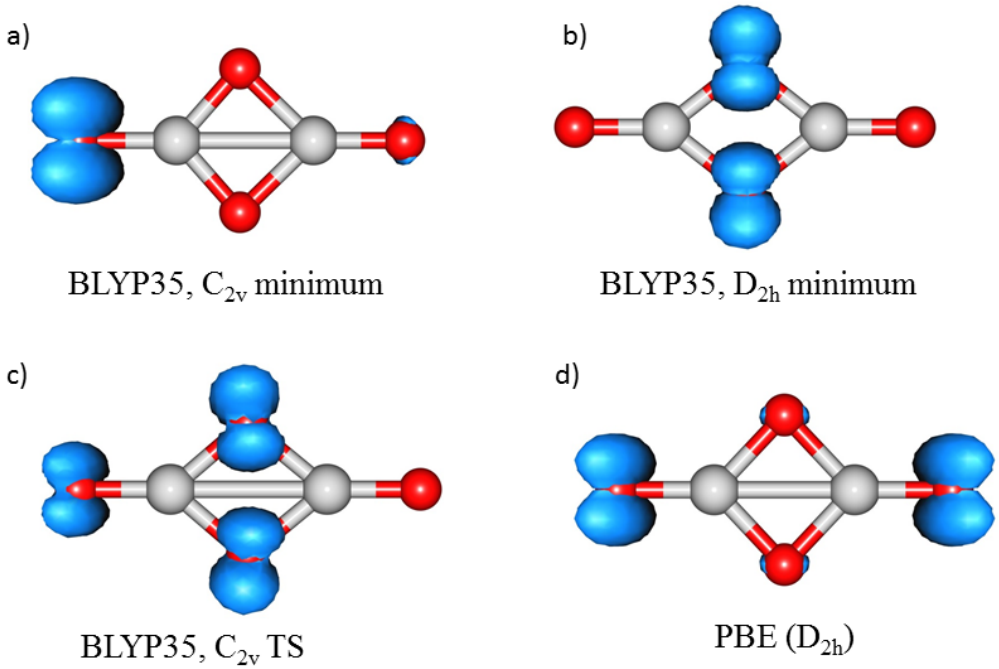

Figure 2. Spin-density isosurfaces (+0.01 a.u.). a) C_{2v} minimum, BLYP35/def2-TZVP; b) D_{2h} minimum BLYP35/def2-TZVP; c) C_{2v} transition state, BLYP35/def2-TZVP; d) optimization PBE/def2-TZVP.

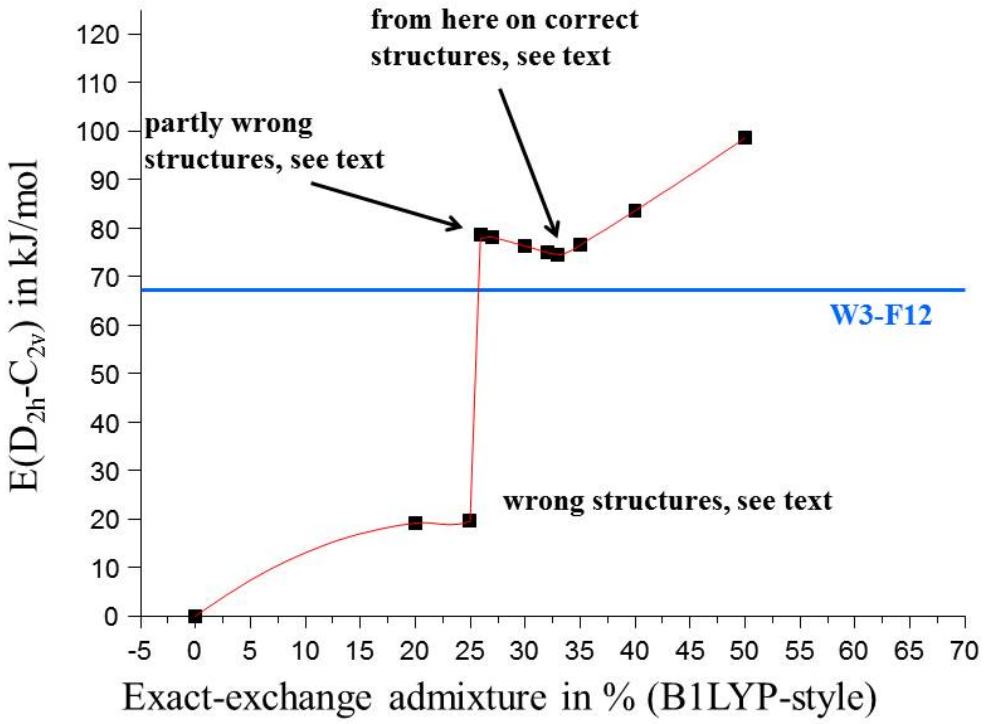

Figure 3. Relative energies for D_{2h} vs. C_{2v} structure optimizations using B1LYP-type global hybrid functionals as function of EXX admixture (in %). The horizontal line shows the benchmark W3-F12 energy. Switching points for structural characteristics are indicated. Cf. Table 2 for numerical data.

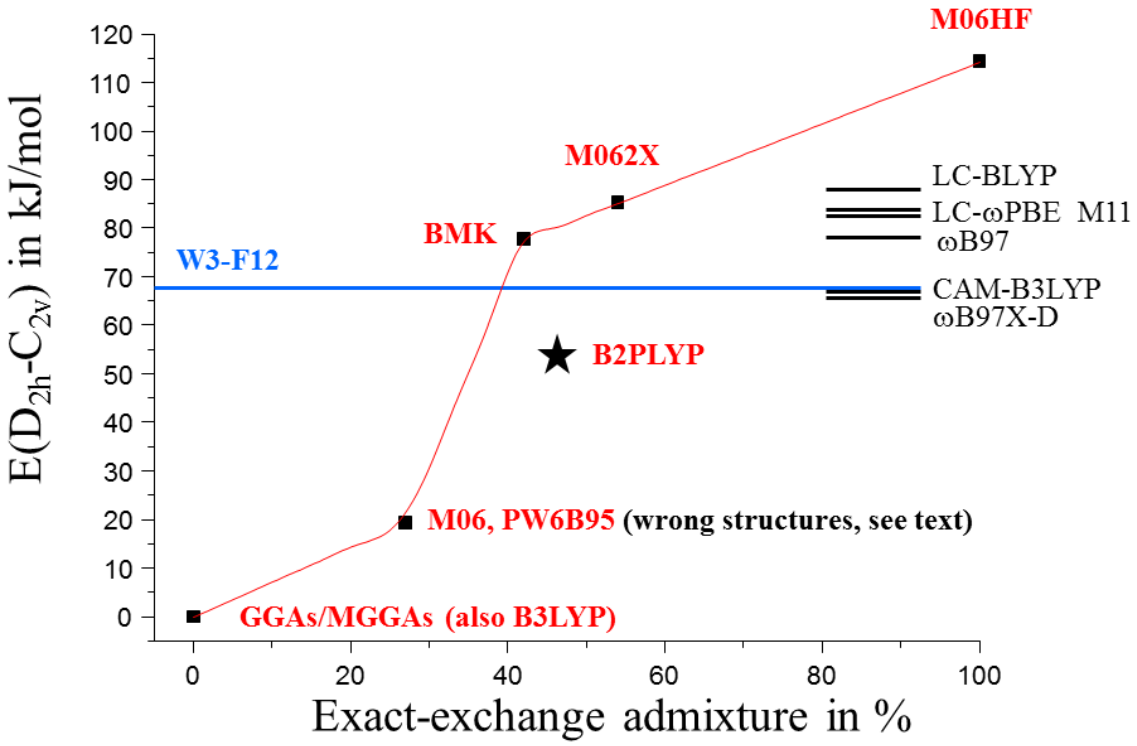

Figure 4. Relative energies of D_{2h} vs. C_{2v} structure optimizations for further functionals. The horizontal line shows the benchmark W3-F12 energy. For global hybrids and the B2PLYP double hybrid, the energies are given as function of EXX admixture. Results with range-separated hybrids are indicated by horizontal lines on the right-hand side. Cf. Table 3 for numerical data.

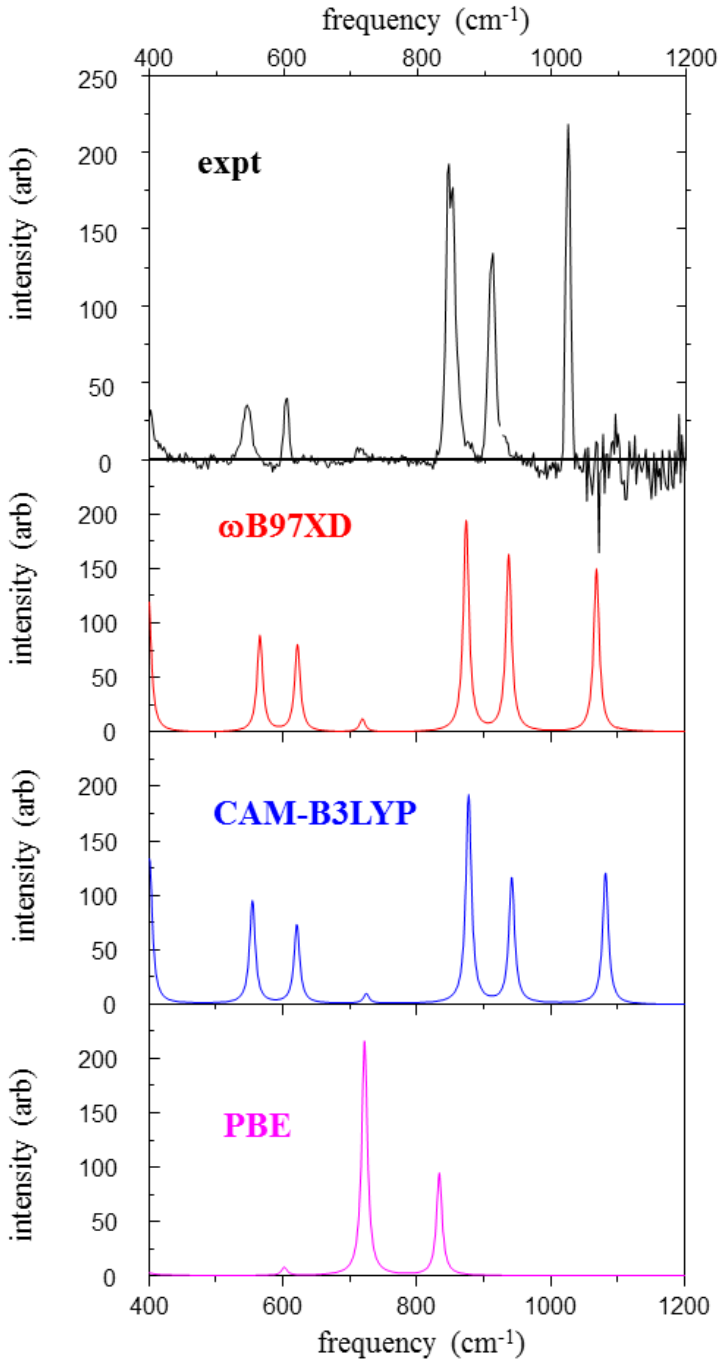

Figure 5. Comparison of IR spectra (broadened by Gaussians with half-width 5 cm^{-1}) computed with different functionals in comparison with the IR-PD spectra of ref. 16. See Table 4 for numerical data. Further vibrational spectra are provided in Figures S1, S2 in Supporting Information.

Table 1. Component breakdown of the W3-F12 energy differences between D_{2h} and C_{2v} minima, and between the C_{2v} transition state and D_{2h} minimum, of $[Al_2O_4]^-$ in kJ/mol

	$\Delta E(D_{2h}-C_{2v})$		$\Delta E(TS-D_{2h})$
ref. struct.	CCSD(T)[f]	BLYP35[g]	BLYP35[g]
HF	208.1	207.2	12.7
ΔCCSD	-117.8	-117.0	-2.6
Δ(T)	-21.2	-20.9	-1.1
ΔT-(T)[a]	1.5	1.5	-2.6
Δ(Q)[b]	-3.0	-3.0	2.1
ΔCV[c]	0.3	0.1	-0.8
CCSD(T)/CBS[d]	69.3	69.5	8.1
CCSDT(Q)/CBS[e]	67.8	67.9	7.6

[a]CCSDT–CCSD(T) energy difference from W3.2 theory. [b]CCSDT(Q)–CCSDT energy difference from W3.2 theory. [c]CCSD(T) core–valence correction. [d]Non-relativistic, all-electron CCSD(T)/CBS energy from W2-F12 theory. [e]Non-relativistic, all-electron CCSDT(Q)/CBS energy from W3-F12 theory. [f]Using CCSD(T)/aug-cc-pVQZ reference structures. [g]Using BLYP35/def2-TZVP reference structures.

Table 2. Relative energies and key structural parameters of D_{2h} vs. C_{2v} minima for B1LYP-type global-hybrid functionals as function of EXX admixture, compared to CCSD(T)/aug-cc-pVQZ benchmark data[a]

functional	ΔE	str. parameters C_{2v}		str. Par. D_{2h}	
		d(AlAl)	Δd(AlO)$_{term}$	d(AlAl)	d(AlO)$_{term}$
BLYP	17.5	2.443	0.000	2.452	1.700
BLYP10	18.4	2.433	0.000	2.438	1.692
BLYP20	19.2	2.429	0.000	2.429	1.685
BLYP25	19.6	2.419	0.000	2.424	1.681
BLYP26	78.7	2.418	0.002	2.793	1.616
BLYP27	78.1	2.418	0.003	2.797	1.615
BLYP30	76.3	2.415	0.007	2.799	1.612
BLYP32	75.0	2.413	0.005	2.799	1.610
BLYP33	74.4	2.416	0.090	2.800	1.610
BLYP35	76.5	2.417	0.119	2.798	1.608
BLYP40	83.6	2.415	0.127	2.798	1.604
BHLYP	98.6	2.407	0.131	2.791	1.598
BLYP35 SVP	69.8	2.433	0.127	2.813	1.611
BLYP35 QZVP	75.3	2.419	0.118	2.799	1.608
CCSD(T)[b]	69.0	2.433	0.121	2.828	1.626

[a]Relative energies in kJ/mol, distances in Å. Def2-TZVP basis results, unless otherwise specified. See Figure 3 for a graphical presentation of the energies. [b]CCSD(T)/aug-cc-pVQZ benchmark data.

Table 3. Relative energies and key structural parameters of D_{2h} vs. C_{2v} minima for further functionals of different classes[a]

	functional	ΔE	str. parameters C_{2v}		str. Par. D_{2h}	
			d(AlAl)	Δd(AlO)$_{term}$	d(AlAl)	d(AlO)$_{term}$
semi-local	PBE	0.0	2.428	0.000	2.428	1.689
	BLYP	0.0	2.443	0.000	2.442	1.692
	M06L	0.0	2.398	0.001	2.399	1.671
	M11L	0.0	2.387	0.001	2.388	1.654
	N12	0.0	2.400	0.000	2.402	1.663
global hybrid	B3LYP	19.2	2.422	0.001	2.425	1.683
	M06	19.4	2.397	0.000	2.402	1.672
	PW6B95	20.3	2.399	0.000	2.405	1.676
	PBE0	80.3	2.407	0.000	2.783	1.615
	PBE0-1/3	77.4	2.407	0.118	2.793	1.608
	BMK	77.8	2.399	0.123	2.786	1.606
	M062X	85.2	2.411	0.126	2.799	1.608
	M06HF	114.3	2.439	0.125	2.828	1.611
range hybrid	CAM-B3LYP	68.7	2.416	0.127	2.802	1.608
	ωB97	77.7	2.428	0.135	2.827	1.611
	ωB97X-D	67.1	2.416	0.128	2.805	1.610
	LC-BLYP	88.4	2.402	0.132	2.796	1.595
	LC-ωPBE	84.5	2.411	0.135	2.780	1.607
	M11	85.3	2.433	0.129	2.822	1.615
	N12SX[b]	0.0	2.407	0.000	2.408	1.667
double hybrid	B2PLYP[c]	54.5	2.427	0.119	2.817	1.624
local hybrid	LSDA, 0.65t[d]	74.9	2.437	0.116	2.828	1.626
CCSD(T)[e]		69.0	2.433	0.121	2.828	1.626

[a]Relative energies in in kJ/mol, distances in Å. def2-TZVP basis results, unless otherwise specified. See Figure 4 for a graphical presentation of the energies. [b]Screened hybrid with 25% EXX at short range and 0% EXX at long range. [c]Deletion of the MP2 energy contributions changes the energy difference to 104.9 kJ/mol. [d]See Computational Details. [e]CCSD(T)/aug-cc-pVQZ benchmark data.

Table 4. Vibrational frequencies and IR intensities computed with different methods (for "correct" C_{2v} structures)[a]

functional	frequency in cm^{-1} (IR intensity in KM/Mole)											
CAM-B3LYP	98	171	247	262	400	402	554	620	724	877	942	1082
	(20)	(36)	(0)	(8)	(133)	(1)	(95)	(73)	(9)	(192)	(116)	(121)
ωB97X-D	99	174	248	266	399	399	565	621	718	873	937	1068
	(20)	(37)	(0)	(6)	(127)	(1)	(88)	(80)	(12)	(194)	(161)	(149)
BLYP35	99	174	248	263	401	403	560	603	714	871	876	1069
	(20)	(38)	(0)	(7)	(19)	(137)	(94)	(10)	(67)	(200)	(139)	(1)
PBE0-1/3	100	173	249	261	399	401	568	599	711	867	873	1067
	(20)	(38)	(0)	(7)	(132)	(27)	(92)	(41)	(107)	(229)	(197)	(0)
BMK	100	179	246	250	396	407	556	631	745	836	925	1077
	(19)	(31)	(9)	(1)	(139)	(5)	(120)	(32)	(0)	(211)	(9)	(48)
M06-2X	101	180	252	266	403	407	566	629	739	900	973	1091
	(20)	(36)	(0)	(8)	(143)	(0)	(100)	(84)	(21)	(202)	(241)	(153)
BHLYP	101	180	255	273	413	417	574	642	750	904	982	1110
	(22)	(39)	(0)	(9)	(0)	(156)	(104)	(86)	(29)	(219)	(264)	(174)
B2PLYP	100	170	240	252	385	395	538	600	707	854	927	1039
	(18)	(32)	(0)	(6)	(110)	(0)	(89)	(83)	(16)	(170)	(189)	(113)
MP2	97	174	243	252	385	396	533	597	704	851	932	1033
	(17)	(32)	(1)	(5)	(111)	(0)	(95)	(95)	(19)	(169)	(274)	(109)
ROCCSD(T)/VTZ[b]	72	160	239	249	385	390	537	601	703	848	925	1030
exp. freq[c]							546	606	711	850	913	1024

References

[1] For some recent reviews see, e.g.: a) Heckmann, A.; Lambert, C. *Angew. Chem. Int.* *51*, 326. b) Day, P.; Hush, N. S.; Clark, R. J. H. *Philos. T. Roy. Soc. A* **2008**, *366*, 5 M. D.; McCleverty, J. A. *J. Chem. Soc., Dalton Trans.* **2002**, 275. d) Brunschwig, C.; Sutin, N. *Chem. Soc. Rev.* **2002**, *31*, 168. e) Demadis, K. D.; Hartshorn, C. M. *Chem. Rev.* **2001**, *101*, 2655. f) Low, P. J. *Dalton Trans.* **2005**, 2821. g) Launay, J. *Soc. Rev.* **2001**, *30*, 386. h) Launay, J.-P. *Coord. Chem. Rev.* **2013**, *257*, 1544. i) C Lapinte, C. *Organomet.* **1996**, *15*, 477. j) Paul, F.; Lapinte, C. *Coord. Chem. Rev.* 431.

[2] Parthey, M.; Kaupp, M. *Chem. Soc. Rev.* **2014**, *43*, 5067.

[3] Robin, M. B.; Day, P. *Adv. Inorg. Chem. Radiochem.* **1967**, *10*, 247.

[4] Renz, M.; Theilacker, K.; Lambert, C.; Kaupp, M. *J. Am. Chem. Soc.* **2009**, *131*, 16 M.; Renz, M.; Parthey, M.; Stolte, M; Würthner, F.; Lambert, C. *Phys. Chem. Che* **2011**, *13*, 16973.

[5] Renz, M.; Kess, M.; Diedenhofen, M.; Klamt, A.; Kaupp, M. *J. Chem. Theor. Com* 4189. Renz, M.; Kaupp, M. *J. Phys. Chem. A* **2012**, *116*, 10629.

[6] Sinnecker, S.; Rajendran, A.; Klamt, A.; Diedenhofen, M.; Neese, F. *J. Phys. Chem* *110*, 2235.

[7] Talipov, M. R.; Boddeda, A.; Timerghazin, Q. K.; Rathore, R. *J. Phys. Chem. C.* **2** 21400.

[8] Kalinowski, J.; Berski, S.; Gordon, A. J. *J. Phys. Chem. A* **2011**, *115*, 13513.

[9] Parthey, M.; Gluyas, J. B. G.; Schauer, P. A.; Yufit, D. S.; Howard, J. A. K.; Kaup P. J. *Chem. Eur. J.* **2013**, *19*, 9780. Parthey, M.; Vincent, K. B.; Renz, M.; Schaue Yufit, D. S.; Howard, J. A. K.; Kaupp, M.; Low, P.J. *Inorg. Chem.* **2014**, *53*, 1544 B.; Zeng, Q.; Parthey, M.; Yufit, D. S.; Howard, J. A. K.; Hartl, F.; Kaupp, M.; Lo *Organometallics* **2013**, *32*, 6022.

[10] Parthey, M.; Gluyas, J. B. G.; Fox, M. A.; Low, P. J.; Kaupp, M. *Chem. Eur. J.* **20**

[11] Sutton, C.; Körzdörfer, T.; Coropceanu, V.; Brédas, J.-L. *J. Phys. Chem. C* **2014**,

[12] Mori, Y. *J. Phys. Org. Chem.* **2014**, *27*, 803.

[13] Yoshida, N.; Ishida, T.; Hirata, F. *J. Phys. Chem. B* **2008**, *112*, 433. Aono, S.; Nak Kurahashi, T.; Fujii, H.; Sakaki, S. *J. Chem. Theor. Comput.* **2014**, *10*, 1062.

[14] See, e.g.: Vydrov, O. A.; Scuseria, G. E. *J. Chem. Phys.* **2006**, *125*, 234109.

[15] See, e.g.: Dehareng, D.; Dive, G.;Moradpour, A. *Int. J. Quant. Chem.* **2000**, *76*, 55 Evangelisti, S.; Leininger, T.; Maynau, D. *J. Comput. Chem.* **2009**, *30*, 83. Fernan

Blancafort, L.; Olivucci, M.; Robb, M. A. *J. Am. Chem. Soc.* **2000**, *122*, 7528. Broo, A.; Larsson, S. *Chem. Phys.* **1992**, *161*, 363. Carissan, Y.; Heully, J.-L.; Alary, F.; Daudey, J.-P. *Inorg. Chem.* **2004**, *43*, 1411.

[16] X. Song, M. Fagiani, S. Gewinner, W. Schöllkopf, K. R. Asmis, F. A. Bischoff, F. Berger, J. Sauer *J. Chem. Phys.*, A16.04.0081R, in press.

[17] See, e.g.: J. To, A.A. Sokol, S. A. French, N. Kaltsoyannis, C. R. A. Catlow *J. Chem. Phys.* **2005**, *122*, 144704; F. Musso, P. Uglienko, X. Solans-Monfort, M. Sodupe *J. Phys. Chem. C* **2010**, *114*, 16430; M. Gerosa, C. Di Valentin, C. E. Bottani, G. Onida, G. Pacchioni *J. Chem. Phys.* **2015**, *143*, 111103, and references cited in these works.

[18] Turbomole V6.4, a development of University of Karlsruhe and Forschungszentrum Karlsruhe GmbH, 1989-2007; Turbomole GmbH, since 2007, available from http://www.turbomole.com; Ahlrichs, R.; Baer, M.; Haeser, M.; Horn, H.; Koelmel, C. *Chem. Phys. Lett.* **1989**, *162*, 165; Treutler, O.; Ahlrichs, R. *J. Chem. Phys.* **1995**, *102*, 346.

[19] *Gaussian 09, Revision A.02, D.01, Frisch, M. J.; et al., Gaussian, Inc., Wallingford CT, 2009.*

[20] MOLPRO is a package of *ab initio* programs written by Werner, H.-J., et al.; MOLPRO 2010.1; University College Cardiff Consultants Limited: Cardiff, U.K., 2010. See also: Werner, H.-J.; Knowles, P. J.; Knizia, G.; Manby, F. R.; Schütz, M. *WIREs Comput. Mol. Sci.* **2012**, *2*, 242, and http:www.molpro. net.

[21] MRCC, a quantum chemical program suite written by Kállay, M.; et al.. See also Rolik, Z.; Szegedy, L.; Ladjánszki, I.; Ladóczki, B. and Kállay, M. *J. Chem. Phys.* **2013**, *139*, 094105, as well as: www.mrcc.hu.

[22] Karton, A.; Martin, J. M. L. *J. Chem. Phys.* **2012**, *136*, 124114.

[23] Karton, A.; Rabinovich, E.; Martin, J. M. L.; Ruscic, B. *J. Chem. Phys.* **2006**, *125*, 144108. Karton, A.; Daon, S.; Martin, J. M. L. *Chem. Phys. Lett.* **2011**, *510*, 165. Karton, A. *WIREs Comput. Mol. Sci.* **2016**, *6*, 29213.

[24] Ten-no, S.; Noga, J. J. *WIREs Comput. Mol. Sci.* **2012**, *2*, 114.

[25] Peterson, K. A.; Feller, D.; Dixon, D. A. *Theor. Chem. Acc.* **2012**, *131*, 1079.

[26] Peterson, K. A.; Adler, T. B.; Werner, H.-J. *J. Chem. Phys.* **2008**, *128*, 084102. Yousaf, K. E.; Peterson, K. *J. Chem. Phys.* **2008**, *129*, 184108.

[27] Yousaf, K. E.; Peterson, K. A. *Chem. Phys. Lett.* **2009**, *476*, 303.

[28] Knizia, G.; Werner, H.-J. *J. Chem. Phys.* **2008**, *128*, 154103.

[29] Adler, T. B.; Knizia, G.; Werner, H.-J. *J. Chem. Phys.* **2007**, *127*, 221106.

[30] Ten-no, S. *Chem. Phys. Lett.* **2004**, *398*, 56. Werner, H.-J.; Adler, T. B.; Manby, F. R. *J. Chem. Phys.* **2007**, *126*, 164102.

[31] Knizia, G.; Adler, T. B.; Werner, H.-J. *J. Chem. Phys.* **2009**, *130*, 054104.

[32] Peterson, K. A.; Dunning, T. H. *J. Chem. Phys.* **2002**, *117*, 10548.

[33] Dunning, T. H. *J. Chem. Phys.* **1989**, *90*, 1007. Kendall, R. A.; Dunning, T. H.; Harrison, R. J. *J. Chem. Phys.* **1992**, *96*, 6796. Dunning, T. H.; Peterson, K. A.; Wilson, A. K. *J. Chem. Phys.* **2001**, 114, 9244.

[34] Halkier, A.; Helgaker, T.; Jørgensen, P.; Klopper, W.; Koch, H.; Olsen, J.; Wilson, A. K. *Chem. Phys. Lett.* **1998**, *286*, 243.

[35] Weigend, F.; Ahlrichs, R. *Phys. Chem. Chem. Phys.* **2005**, *7*, 3297.

[36] Becke, A. D. *J. Chem. Phys.* **1993**, *98*, 1372.

[37] Adamo, C.; Barone, V. *Chem. Phys. Lett.* **1997**, *274*, 242.

[38] Schäfer, A.; Horn, H.; Ahlrichs, R. *J. Chem. Phys.* **1992**, *97*, 2571.

[39] Fukui, K. *Acc. Chem. Res*. **1981**, *14*, 363. Hratchian, H. P. Schlegel, H. B. *J. Chem. Theor. Comput.* **2005**, *1*, 61.

[40] Zhao, Y.; Truhlar, D. G. *J. Phys. Chem. A* **2005**, *109*, 5656.

[41] Goerigk, L.; Grimme, S. *Phys. Chem. Chem. Phys.* **2011**, *13*, 6670.

[42] Perdew, J. P.; Wang, Y. *Phys. Rev. B* **1992**, *45*, 13244.

[43] Bahmann, H.; Rodenberg, A.; Arbuznikov, A. V.; Kaupp, M. *J. Chem. Phys.* **2007***, 126,* 011103. Kaupp, M.; Bahmann, H.; Arbuznikov, A.V. *J. Chem. Phys.* **2007**, *127*, 194102.

[44] Arbuznikov, A. V.; Kaupp, M. *J. Chem. Phys.* **2014**, *141*, 204101; Theilacker, K.; Arbuznikov, A. V.; Kaupp, M. *Mol. Phys.* **2016**, *114*, 1118. Maier, T. M.; Haasler, M.; Arbuznikov, A.V.; Kaupp, M. *Phys. Chem. Chem. Phys.*, 2016, DOI: 10.1039/C6CP00990E.

[45] Bahmann, H.;. Kaupp, M. *J. Chem. Theor. Comput.* **2015**, *11*, 1540.

[46] Becke, A. D. *Phys. Rev. A* **1988**, *38*, 3098. Lee, C.; Yang, W.; Parr, R. G. *Phys. Rev. B* **1988**, *37*, 785.

[47] Perdew, J. P.; Burke, K.; Ernzerhof, M. *Phys. Rev. Lett.* **1996**, *77*, 3865.

[48] Zhao, Y.; Truhlar, D. G. *J. Chem. Phys.* **2006**, *125*, 194101.

[49] Peverati, R.; Truhlar, D. G. *J. Phys. Chem. Lett.* **2012**, *3*, 117.

[50] Peverati, R.; Truhlar, D. G. *J. Chem. Theor. Comput.* **2012**, *8*, 2310.

[51] Becke, A. D. *J. Chem. Phys.* **1993**, *98*, 5648. Stephens, P. J.; Devlin, F. J.; Chabalowski, C. F.; Frisch, M. J. *J. Phys. Chem.* **1994**, *98*, 11623.

[52] Adamo, C.; Barone, V. *J. Chem. Phys.* **1999**, *110*, 6158.

[53] Guido, C. A.; Brémond, E.; Adamo, C.; Cortona, P. *J. Chem. Phys.* **2013**, *138*, 021104.

[54] Boese, A. D.; Martin, J. M. L. *J. Chem. Phys.* **2004**, *121*, 3405.

[55] Zhao, Y.; Truhlar, D. G. *Theor. Chem. Acc.* **2008**, *120*, 215.

[56] Zhao, Y. Truhlar, D. G. *J. Phys. Chem. A.* **2006**, *110*, 13126.

[57] Yanai, T.; Tew, D. P.; Handy, N. C. *Chem. Phys. Lett.* **2004**, *393*, 51.

[58] Chai, J.-D.; Head-Gordon, M. *Phys. Chem. Chem. Phys.* **2008**, *10*, 6615.

[59] Chai, J. D.; Head-Gordon, M. *J. Chem. Phys.* **2008**, *128*, 084106.

[60] Iikura, H.; Tsuneda, T.; Yanai, T.; Hirao, K. *J. Chem. Phys.* **2001**, *115*, 3540.

[61] Vydrov, O. A.; Heyd, J.; Krukau, A. V.; Scuseria, G. E. *J. Chem. Phys.* **2006**, *125*, 074106. Vydrov, O. A.; Scuseria, G. E.; Perdew, J. P. *J. Chem. Phys.* **2007**, *126*, 154109.

[62] Peverati, R.; Truhlar, D. G. *J. Phys. Chem. Lett.* **2011**, *2*, 2810.

[63] Peverati, R.; Truhlar, D. G. *Phys. Chem. Chem. Phys.* **2012**, *14*, 16187.

[64] Schwabe, T.; Grimme, S. *Phys. Chem. Chem. Phys.* **2007**, *9*, 3397.

[65] http://www.chemcraftprog.com.

[66] Reed, A. E.; Weinstock, R. B.; Weinhold, F. *J. Chem. Phys.* **1985**, *83*, 735.

[67] See, e.g.: Fox, M. A.; Le Guennic, B.; Roberts, R. L.; Brue, D. A.; Yufit, D. S.; Howard, J. A. K.; Manca, G.; Halet, J.-F.; Hartl, F.; Low, P. J. *J. Am. Chem. Soc.* **2011**, *133*, 18433.

[68] Hamann, B.; Chen, C.; Flörke, U.; Hauptmann, R.; Bill, E.; Sinnecker, S.; Henkel, G. *Angew. Chem. Int. Ed.* **2006**, *45*, 8245. Aullón, G.; Hamidi, M.; Lledós, A.; Alvarez, S. *Inorg. Chem.* **2004**, *43*, 3702.

[69] Gandon, V.; Bourg, J.-B.; Tham, F. S.; Schoeller, W.; Bertrand, G. *Angew. Chem., Int. Ed.* **2008**, *47*, 155.

[70] See, e.g.: N. Dietl, M. Schlangen, H. Schwarz *Angew. Chem., Int. Ed. Engl.* **2012**, *51*, 5544, and references therein.

[71] Janssen, C. L.; Nielsen, I. M. B. *Chem. Phys. Lett.* **1998**, *290*, 423.

[72] Jiang, W.; DeYonker, N. J.; Determan, J. J.; Wilson, A. K. *J. Phys. Chem. A* **2012**, *116*, 870.

[73] Korth, M.; Grimme, S. *J. Chem. Theor. Comput.* **2009**, *5*, 993.

[74] Feller, D.; Peterson, K. A. *J. Chem. Phys.* **2007**, *126*, 114105.

[75] Munzarová, M.; Kaupp, M. *J. Phys. Chem. A* **1999**, *103,* 9966.

[76] Krukau, A. V.; Vydrov, O. A.; Izmaylov, A. F.; Scuseria, G. E. *J. Chem. Phys.* **2006**, *125*, 224106.

[77] Cortona, P. *J. Chem. Phys.* **2012**, *136*, 086101.

[78] Arbuznikov, A. V.; Kaupp, M. *J. Chem. Phys.* **2012**, *136*, 014111.